Non-Gaussian quantum states of a multimode light field

Young-Sik Ra, Adrien Dufour, Mattia Walschaers, Clément Jacquard, Thibault Michel, Claude Fabre, Nicolas Treps

Non-Gaussian quantum states of a multimode light field

Young-Sik Ra,[1,2,*] Adrien Dufour,[1] Mattia Walschaers,[1]
Clément Jacquard,[1] Thibault Michel,[1,3] Claude Fabre,[1] and Nicolas Treps[1]

[1]*Laboratoire Kastler Brossel, Sorbonne Université, CNRS, ENS-PSL Research University, Collège de France; 4 place Jussieu, 75252 Paris, France*

[2]*Department of Physics, Korea Advanced Institute of Science and Technology (KAIST), Daejeon 34141, Korea*

[3]*Center for Quantum Computation and Communication Technology, Department of Quantum Science, The Australian National University, Canberra, ACT 0200, Australia*

(Dated: September 29, 2019)

* youngsikra@gmail.com

Advanced quantum technologies require scalable and controllable quantum resources [1, 2]. Gaussian states of multimode light such as squeezed states and cluster states are scalable quantum systems [3–5], which can be generated on demand. However, non-Gaussian features are indispensable in many quantum protocols, especially to reach a quantum computational advantage [6]. Embodying non-Gaussianity in a multimode quantum state remains a challenge as non-Gaussian operations generally cannot maintain coherence among multiple modes. Here, we generate non-Gaussian quantum states of a multimode light field by removing a single photon in a mode-selective manner from a Gaussian state [7]. The selectivity and the controllability of the mode(s) for this photon subtraction process make it possible to extend the non-Gaussianity of a quantum state to the multimode regime, which has been a main obstacle for scalable quantum information processing. To highlight the potential for continuous-variable quantum technologies, we first demonstrate the capability to generate negativity of the Wigner function in a controlled mode. Subsequently, we explore the interplay between non-Gaussianity and quantum entanglement, and verify a theoretical prediction [8] about the propagation of non-Gaussianity along the nodes of photon-subtracted cluster states. Our results demonstrate large-scale non-Gaussianity with an unprecedented flexibility, while ensuring the compatibility with quantum information protocols. This range of features makes our approach ideal to explore the physics of non-Gaussian entanglement [9, 10], and to develop quantum protocols, ranging from quantum computing [11, 12], over entanglement distillation [13], to quantum simulations [14].

Our starting point is a multimode squeezed vacuum state of light, a basic quantum resource for continuous-variable quantum technologies such as quantum-enhanced sensing [15] and deterministic quantum state teleportation [16]. Recent technological advances have extended the generation and control of squeezed vacuum from a single mode to multiple modes, which enables a deterministic generation of large-scale multipartite entangled states [3–5]. However, such quantum states intrinsically exhibit Gaussian statistics in electric field quadrature measurements. These Gaussian states have limitations to reach quantum advantages [6], e.g., entanglement distillation [13] and universal quantum computing [11, 12]. Non-Gaussian quantum states, on the other hand, are connected to exotic quantum fea-

tures such as contextuality, which goes hand in hand with negative values of the Wigner function [17].

The hybrid approach, which combines continuous-variable and discrete-variable quantum information processing, provides a solution [1]. Subtracting/adding a discrete number of photons [18] can generate non-Gaussian states such as a local or non-local superposition of coherent states [19–23] and hybrid entanglement [24, 25]. Hitherto, this approach has only been successfully applied to a single- or two-mode quantum state, and the extension to highly multimode quantum states remains challenging due to the arduous task of maintaining coherence among multiple modes [7].

To exploit the full potential of the large-scale entangled states that are generated by our source [4], it is essential that the hybrid approach is made compatible with multimode quantum states. The concept of our experiment is illustrated in Fig. 1(a). We choose photon subtraction as it generally leads to a stronger increase in entanglement than photon addition and is simpler to implement [26]. If we call $\hat{\rho}$ the density operator of an input multimode quantum state, the output state $\hat{\rho}^-$ by a photon subtraction operator $\hat{A}$ becomes

$$\hat{\rho}^- \propto \hat{A}\hat{\rho}\hat{A}^\dagger, \quad \text{where } \hat{A} = \sum_{k=0} c_k \hat{a}_k. \tag{1}$$

c_k are complex numbers normalized as $\sum |c_k|^2 = 1$, and $\hat{a}_k$ is the annihilation operator for mode k. Note that $\hat{A}$ is, in general, an annihilation operator in an arbitrary mode. The ability to experimentally control both the c_k coefficient and the multimode resource $\hat{\rho}$ is the key to tailor non-Gaussian multimode states and to achieve non-Gaussian entanglement for building non-Gaussian quantum networks [8, 27].

In our experiment, the controlled generation of non-Gaussian multimode quantum states is performed using quantum frequency combs as a resource. Figure 1(b) shows the experimental setup, whose details are presented in Methods. The optical modes in which we implement Eq. (1) are time-frequency modes [28]. The interest of these modes is that they are co-propagating in the same transverse mode, allowing for a large multimode quantum resource to keep its coherence and for the access to arbitrary superpositions of modes without constructing an interferometer. We populate these modes with a highly multimode Gaussian state through a parametric down conversion process [4]. Tailoring the measurement mode basis allows for the generation of versatile multipartite entangled states [29]. We combine this resource with a time-frequency mode-dependent photon subtractor to de-Gaussify such

multimode Gaussian states.

More specifically, our multimode Gaussian resource $\hat{\rho}$ is a set of independent squeezed vacua whose eigenmodes are conveniently approximated by time-frequency Hermite-Gaussian modes HG_k. In order to implement the concepts of Eq. (1), we associate these modes with the annihilation operators $\hat{a}_k$. Hence, it remains to control the c_k coefficients for the photon subtraction. As shown in Fig. 1(b), this is implemented through a mode-selective sum-frequency generation between the Gaussian resource $\hat{\rho}$ and a gate beam [30]. The non-linear interaction is designed such that pulse-shaping the gate allows for the control of the mode of photon subtraction [28]. Finally, detection of a single photon in the up-converted beam heralds the subtraction of a photon in the desired mode from the Gaussian resource. The intensity of the gate governs the efficiency of the operation, and hence the heralding probability.

To characterize the resulting non-Gaussian multimode quantum state, we employ a homodyne detection that can control the mode of measurement by pulse-shaping the local oscillator. By virtue of these homodyne measurements, we show that our setup can generate a wide range of quantum states with key properties for the development of quantum technologies: negativity of the Wigner function on the one hand, and non-Gaussian entangled states on the other hand.

In the first column of Fig. 2(a), we first measure the input multimode squeezed vacua without photon subtraction (i.e., no gate field is applied). As expected, the measured state exhibits Gaussian distribution. This behavior changes drastically in the second column, where a single photon is subtracted in HG_0: the multimode Wigner function becomes negative. More specifically, the reconstructed Wigner function in HG_0 reaches negative values (explicitly highlighted by W_0), while the Wigner functions in the other modes remain Gaussian, thus demonstrating the mode-selective operation of the photon subtractor. Similarly, when a photon is subtracted in HG_1, we observe a non-Gaussian Wigner function only in HG_1. Due to a larger optical loss in the input state for higher order modes than in HG_0, the negativity of the Wigner function is unveiled only upon loss-correction, as shown in Extended Data Fig. 1. Analogous results are obtained for the subtraction of a photon in the HG_2 mode, but due to higher losses the resulting Wigner function remains positive. The high quality of the photon subtraction process is emphasized in Fig. 2 by the high fidelity

(F) between experimental results and the ideal Wigner functions calculated by subtracting a photon from the corresponding input state.

Furthermore, the versatility of the experimental setup allows for the computer controlled subtraction of a photon in an arbitrary superposition of modes from a multimode quantum state. As an example, we subtract a photon in a superposition of HG_0 and HG_1 modes, $\mathrm{HG}_0 - i\mathrm{HG}_1$. We observe that the photon subtraction induces negativity in the Wigner function for this mode (first row of Fig. 2(b)). On the other hand, in the orthogonal mode $\mathrm{HG}_0 + i\mathrm{HG}_1$, a Gaussian Wigner function is obtained, and in a partially overlapping mode $i\mathrm{HG}_1$, an intermediate situation is obtained as expected, see Extended Data Fig. 2. When we subtract a photon in a superposition of three modes $\mathrm{HG}_0 + i\mathrm{HG}_1 + \mathrm{HG}_2$, we similarly observe a non-Gaussian Wigner function in the same superposed modes (second row of Fig. 2(b)), which remains positive due to the impurity of the input state.

The flexibility of the setup allows us to extend photon subtraction to entangled input states. We first investigate an Einstein-Podolsky-Rosen (EPR) entangled state, which exhibits quantum correlations between two superposed modes: $\mathrm{EPR}_0 = \mathrm{HG}_0 + \mathrm{HG}_1$ and $\mathrm{EPR}_1 = \mathrm{HG}_0 - \mathrm{HG}_1$ (see Methods). The last two rows in Fig. 2(b) show the experimentally obtained Wigner functions. Without photon subtraction, the reduced quantum state in each of EPR_0 and EPR_1 is a thermal state as expected. When a photon is subtracted in EPR_0, the introduced non-Gaussian characteristics—including negativity of the Wigner function—appear in the other mode (EPR_1) with almost no effect on the mode in which the photon is actually subtracted. A completely analogous effect is observed when the photon is subtracted in EPR_1. In striking contrast with the aforementioned separable input state, the effect of photon subtraction on an entangled state is not localized but is transferred to another mode.

In addition to generating Wigner functions that reach negative values, the results for these EPR state show that our setup is an ideal toolbox to study the interplay between non-Gaussianity and quantum entanglement. Cluster states, which form the backbone of measurement-based quantum computation [12], are a well-suited class of states to explore the rich entanglement structures in our quantum frequency combs [29]. Upon photon subtraction in a given node and due to this cluster like correlation patterns, the non-Gaussian features will not remain concentrated in a single node but will spread among those linked to the photon-subtracted node [8]. This implies that the negativity of the multimode Wigner

function can generally not be retrieved from single-mode measurements (not even in the fully idealized pure state scenario). However, this interplay between non-Gaussianity and entanglement can be tested by measuring the propagation of non-Gaussian features through the cluster states using easily accessible higher order statistical properties such as the kurtosis and directly compared with theoretical predictions [8].

We experimentally realize a four-mode linear cluster (LC) state and a four-mode square cluster (SC) state (see Methods), where we denote the four modes of the linear one as LC_k ($k = 0, 1, 2, 3$) and the square one as SC_k ($k = 0, 1, 2, 3$). We quantify the non-Gaussianity in each mode by evaluating the phase-averaged excess kurtosis (to compare with the kurtosis of 3 by a Gaussian distribution). This is obtained from the quadrature measurement outcomes $x_1, x_2, ..., x_S$ where the measurement phase is randomized:

$$K_{\mathrm{ex}} = \frac{\frac{1}{S}\sum_{s=1}^{S} x_s^4}{\left(\frac{1}{S}\sum_{s=1}^{S} x_s^2\right)^2} - 3 \tag{2}$$

For a quantum state with zero mean ($\langle\hat{a}\rangle = \langle\hat{a}^\dagger\rangle = 0$), which corresponds to all the quantum states in our experiment, a Gaussian state always exhibits $K_{\mathrm{ex}} \geq 0$, thus $K_{\mathrm{ex}} < 0$ indicates a non-Gaussian state. Figure 3 shows excess kurtosis of the generated states. For the linear cluster state, excess kurtosis in each mode is initially close to zero. When a photon is subtracted in LC_3, it is LC_2 in which excess kurtosis becomes highly negative (i.e. non-Gaussian) while those in the other modes remain close to zero. For photon subtraction in LC_2, only LC_3 exhibits a significant negativity. We can concentrate more non-Gaussianity in LC_3 by subtracting a photon in a superposition of four modes, as shown in the last figure of Fig. 3(a). For the square cluster state, excess kurtosis without photon subtraction is close to zero in each mode. Photon subtraction in SC_0, however, does not affect the distributions in its nearby modes (SC_1 and SC_3) much, but it introduces non-Gaussianity mostly in SC_2 which is two steps away from the mode of photon subtraction. This effect was predicted in [8] and we note an excellent agreement between the measured kurtosis values and the theoretical values calculated from the measured input Gaussian states. Hence, even though the obtained values for the excess kurtosis are consistent with reported values for photon-subtracted thermal states [31], the hallmark of non-Gaussian correlation lies in the way that these non-Gaussian effects propagate through the nodes of the cluster state.

In the future, our approach can be used to generate a broader class of non-Gaussian states by subtracting multiple photons, either via a sequence of subtractors or by replacing

the single-photon detector with a number-resolved subtraction scheme. In such a scenario, the success probability of the heralding will be a limiting factor, which could be significantly improved by a repeat-until-success scheme [32]. More generally, the availability of non-Gaussian multimode states will stimulate fundamental studies on non-Gaussian entanglement [10, 33] and quantumness [34, 35] by going beyond the Gaussian realm, as well as applications in quantum technologies [11–13, 36]. In particular, the observed nontrivial interplay between photon subtraction and cluster states, confirming recent theoretical predictions [8], provides an ideal avenue for future experimental studies of non-Gaussian entanglement and its applications.

ACKNOWLEDGEMENTS

This work is supported by the French National Research Agency projects COMB and SPOCQ, the European Union Grant QCUMbER (no. 665148). C.F. and N.T. are members of the Institut Universitaire de France. Y.-S.R. acknowledges support from the European Commission through Marie Skłodowska-Curie actions (no. 708201) and the National Research Foundation of Korea (NRF) funded by the Ministry of Education (NRF-2018R1A6A3A03012129) and the Ministry of Science and ICT (NRF-2019R1C1C1005196). M.W. acknowledges funding through research fellowship WA 3969/2-1 from the German Research Foundation (DFG).

AUTHOR CONTRIBUTIONS

Y.-S.R. and A.D. conducted the experiments with help from C.J. and T.M. Y.-S.R. and M.W. analyzed the data. M.W. developed the theoretical model. Y.-S.R., M.W and N.T. wrote the manuscript with input from all authors. C.F. and N.T. supervised the project. All authors contributed to scientific discussions.

COMPETING INTERESTS

The authors declare no competing interests.

---

[1] Andersen, U. L., Neergaard-Nielsen, J. S., Van Loock, P. and Furusawa, A., Hybrid discrete- and continuous-variable quantum information, *Nat. Phys.* **11**, 713–719 (2015).

[2] Biamonte, J. *et al.*, Quantum machine learning, *Nature* **549**, 195–202 (2017).

[3] Yokoyama, S. *et al.*, Ultra-large-scale continuous-variable cluster states multiplexed in the time domain, *Nat. Photonics* **7**, 982–986 (2013).

[4] Roslund, J., Medeiros de Araújo, R., Jiang, S., Fabre, C. and Treps, N., Wavelength-multiplexed quantum networks with ultrafast frequency combs, *Nat. Photonics* **8**, 109–112 (2014).

[5] Chen, M., Menicucci, N. C. and Pfister, O., Experimental Realization of Multipartite Entanglement of 60 Modes of a Quantum Optical Frequency Comb, *Phys. Rev. Lett.* **112**, 120505 (2014).

[6] Mari, A. and Eisert, J., Positive Wigner Functions Render Classical Simulation of Quantum Computation Efficient, *Phys. Rev. Lett.* **109**, 230503 (2012).

[7] Averchenko, V., Jacquard, C., Thiel, V., Fabre, C. and Treps, N., Multimode theory of single-photon subtraction, *New J. Phys.* **18**, 083042 (2016).

[8] Walschaers, M., Sarkar, S., Parigi, V. and Treps, N., Tailoring Non-Gaussian Continuous-Variable Graph States, *Phys. Rev. Lett.* **121**, 220501 (2018).

[9] Valido, A. A., Levi, F. and Mintert, F., Hierarchies of multipartite entanglement for continuous-variable states, *Phys. Rev. A* **90**, 052321 (2014).

[10] Park, K., Marek, P. and Filip, R., Conditional superpositions of Gaussian operations on different modes of light, *Phys. Rev. A* **91**, 033814 (2015).

[11] Lloyd, S. and Braunstein, S. L., Quantum computation over continuous variables, *Phys. Rev. Lett.* **82**, 1784–1787 (1999).

[12] Menicucci, N. C. *et al.*, Universal quantum computation with continuous-variable cluster states, *Phys. Rev. Lett.* **97**, 110501 (2006).

[13] Eisert, J., Scheel, S. and Plenio, M. B., Distilling Gaussian States with Gaussian Operations is Impossible, *Phys. Rev. Lett.* **89**, 137903 (2002).

[14] Banchi, L., Fingerhuth, M., Babej, T., Ing, C. and Arrazola, J. M., Molecular Docking with Gaussian Boson Sampling, Preprint at https://arxiv.org/abs/1902.00462 (2019).

[15] Aasi, J. *et al.*, Enhanced sensitivity of the LIGO gravitational wave detector by using squeezed states of light, *Nat. Photonics* **7**, 613–619 (2013).

[16] Takeda, S., Mizuta, T., Fuwa, M., Van Loock, P. and Furusawa, A., Deterministic quantum teleportation of photonic quantum bits by a hybrid technique, *Nature* **500**, 315–318 (2013).

[17] Spekkens, R. W., Negativity and Contextuality are Equivalent Notions of Nonclassicality, *Phys. Rev. Lett.* **101**, 020401 (2008).

[18] Wenger, J., Tualle-Brouri, R. and Grangier, P., Non-Gaussian statistics from individual pulses of squeezed light, *Phys. Rev. Lett.* **92**, 153601 (2004).

[19] Ourjoumtsev, A., Tualle-Brouri, R., Laurat, J. and Grangier, P., Generating optical Schrödinger kittens for quantum information processing, *Science (New York, NY)* **312**, 83–86 (2006).

[20] Ourjoumtsev, A., Ferreyrol, F., Tualle-Brouri, R. and Grangier, P., Preparation of non-local superpositions of quasi-classical light states, *Nat. Phys.* **5**, 189–192 (2009).

[21] Sychev, D. V. *et al.*, Enlargement of optical Schrödinger's cat states, *Nat. Photonics* **11**, 379–382 (2017).

[22] Serikawa, T. *et al.*, Generation of a Cat State in an Optical Sideband, *Phys. Rev. Lett.* **121**, 143602 (2018).

[23] Biagi, N., Costanzo, L. S., Bellini, M. and Zavatta, A., Entangling macroscopic light states by delocalized photon addition, Preprint at https://arxiv.org/abs/1811.10466 (2018).

[24] Jeong, H. *et al.*, Generation of hybrid entanglement of light, *Nat. Photonics* **8**, 564–569 (2014).

[25] Morin, O. *et al.*, Remote creation of hybrid entanglement between particle-like and wave-like optical qubits, *Nat. Photonics* **8**, 570–574 (2014).

[26] Das, T., Prabhu, R., Sen De, A. and Sen, U., Superiority of photon subtraction to addition for entanglement in a multimode squeezed vacuum, *Phys. Rev. A* **93**, 052313 (2016).

[27] Walschaers, M., Fabre, C., Parigi, V. and Treps, N., Entanglement and Wigner Function Negativity of Multimode Non-Gaussian States, *Phys. Rev. Lett.* **119**, 183601 (2017).

[28] Ansari, V., Donohue, J. M., Brecht, B. and Silberhorn, C., Tailoring nonlinear processes for quantum optics with pulsed temporal-mode encodings, *Optica* **5**, 534–550 (2018).

[29] Cai, Y. *et al.*, Multimode entanglement in reconfigurable graph states using optical frequency combs, *Nat. Commun.* **8**, 15645 (2017).

[30] Ra, Y.-S., Jacquard, C., Dufour, A., Fabre, C. and Treps, N., Tomography of a Mode-Tunable Coherent Single-Photon Subtractor, *Phys. Rev. X* **7**, 031012 (2017).

[31] Bogdanov, Y. I. *et al.*, Multiphoton subtracted thermal states: Description, preparation, and reconstruction, *Phys. Rev. A* **96**, 063803 (2017).

[32] Marek, P., Provazník, J. and Filip, R., Loop-based subtraction of a single photon from a traveling beam of light, *Opt. Express* **26**, 29837–29847 (2018).

[33] Katamadze, K. G., Avosopiants, G. V., Bogdanov, Y. I. and Kulik, S. P., How quantum is the "quantum vampire" effect?: Testing with thermal light, *Optica* **5**, 723–726 (2018).

[34] Ježek, M. *et al.*, Experimental test of the strongly nonclassical character of a noisy squeezed single-photon state, *Phys. Rev. A* **86**, 043813 (2012).

[35] Albarelli, F., Genoni, M. G., Paris, M. G. A. and Ferraro, A., Resource theory of quantum non-Gaussianity and Wigner negativity, *Phys. Rev. A* **98**, 052350 (2018).

[36] Plick, W. N., Arzani, F., Treps, N., Diamanti, E. and Markham, D., Violating Bell inequalities with entangled optical frequency combs and multipixel homodyne detection, *Phys. Rev. A* **98**, 062101 (2018).

[37] Neergaard-Nielsen, J., Nielsen, B., Hettich, C., Molmer, K. and Polzik, E., Generation of a Superposition of Odd Photon Number States for Quantum Information Networks, *Phys. Rev. Lett.* **97**, 083604 (2006).

[38] Duan, L.-M., Giedke, G., Cirac, J. I. and Zoller, P., Inseparability Criterion for Continuous Variable Systems, *Phys. Rev. Lett.* **84**, 2722–2725 (2000).

[39] Simon, R., Peres-Horodecki Separability Criterion for Continuous Variable Systems, *Phys. Rev. Lett.* **84**, 2726–2729 (2000).

[40] Bowen, W. P., Schnabel, R., Lam, P. K. and Ralph, T. C., Experimental Investigation of Criteria for Continuous Variable Entanglement, *Phys. Rev. Lett.* **90**, 043601 (2003).

[41] van Loock, P., Weedbrook, C. and Gu, M., Building Gaussian cluster states by linear optics, *Phys. Rev. A* **76**, 032321 (2007).

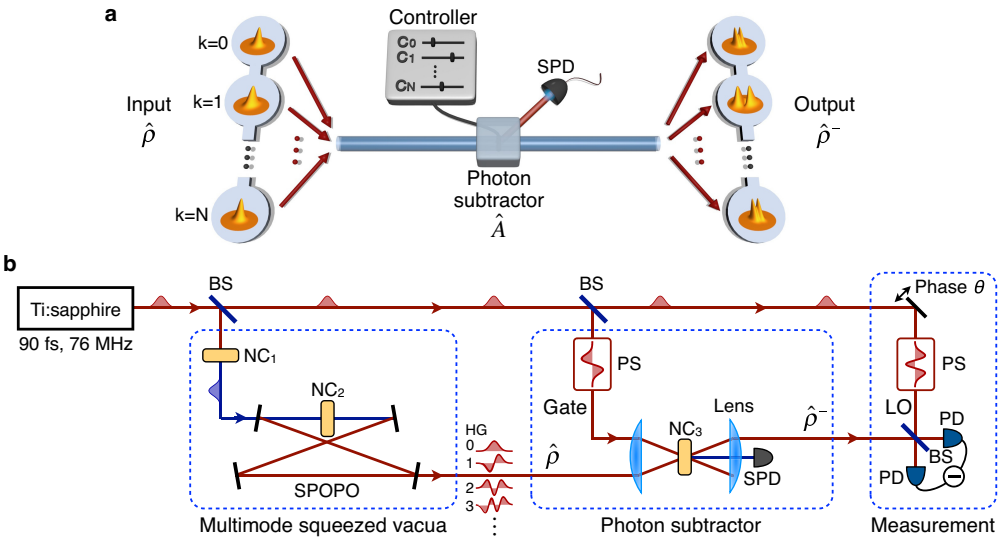

FIG. 1. **Mode-selective photon subtraction from a multimode quantum state.** (a) Concept. Input is a beam containing a Gaussian multimode quantum state $\hat{\rho}$, which can be, in general, a multipartite entangled state. From the input state, we subtract a photon in a specific mode or in a coherent superposition of multiple modes by controlling the complex coefficient c_k for each mode k. This process, described by an annihilation operator $\hat{A}$ in Eq. (1), is heralded by a registration of a photon at the single-photon detector (SPD). As a result, the output beam contains a non-Gaussian multimode quantum state $\hat{\rho}^-$. The inset inside each circle is the Wigner function of the reduced quantum state in the associated mode. (b) Experimental setup. A Ti:sapphire laser produces a beam made of a train of femtosecond pulses, which splits into three beams. One beam is up-converted via second harmonic generation in a second-order nonlinear crystal (NC_1), and then, pumps NC_2 for a parametric down-conversion process. Synchronously pumped optical parametric oscillator (SPOPO) amplifies the process, which generates twelve-mode squeezed vacua in well-defined time-frequency modes. Another beam is used as a gate for the photon subtractor, and its time-frequency mode is engineered by a pulse shaper (PS). Inside NC_3, sum-frequency-interaction between the gate and the multimode squeezed vacua generates an up-converted beam, which is detected by SPD. A photon registration in SPD heralds photon subtraction from the multimode squeezed vacua. The resulting multimode quantum state is measured by homodyne detection with a time-frequency-engineered local oscillator (LO) using another PS. PD: photo diode; BS: beam splitter; θ: phase of LO.

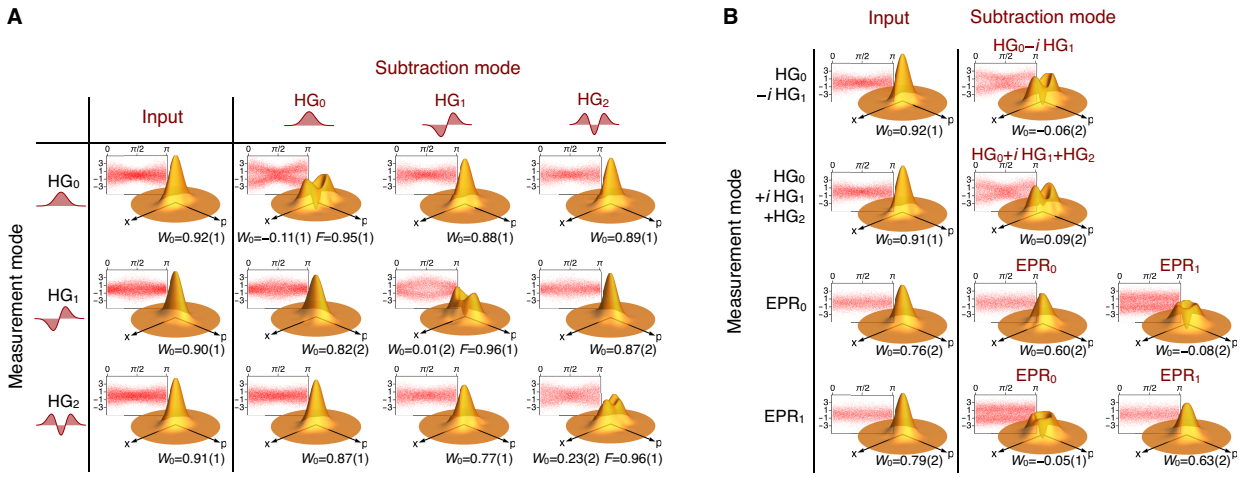

FIG. 2. **Wigner function reconstructed from experimental data.** For a multimode quantum state, photon subtraction and measurement are conducted in (a) HG modes or in (b) superpositions of HG modes. The Wigner function of each mode is represented in the phase space of x and p axes, which are associated with quadrature operators $\hat{x} = \hat{a} + \hat{a}^\dagger$ and $\hat{p} = (\hat{a} - \hat{a}^\dagger)/i$, respectively. The inset behind each Wigner function shows the experimentally obtained quadrature outcomes, where the horizontal and vertical axes represent the phase of local oscillator and a quadrature outcome, respectively; the quadrature outcome of one corresponds to the variance of the vacuum fluctuation. No correction of optical losses is made; for the results by optical loss correction, see Extended Data Fig. 1. $W_0 = 2\pi W(0,0)$ is the value of a normalized Wigner function at the origin, and F is the fidelity between an experimental Wigner function and the Wigner function by the ideal photon subtraction to the input state of the corresponding mode. Purities of the Wigner functions in (a), compared with the cases of the ideal photon subtraction, are presented in Extended Data Tab. 1. For measurements in modes EPR_0 and EPR_1, the phase of a quadrature outcome is randomized since the associated quantum state is phase insensitive. Errors noted in parentheses are one standard deviations calculated by bootstrapping.

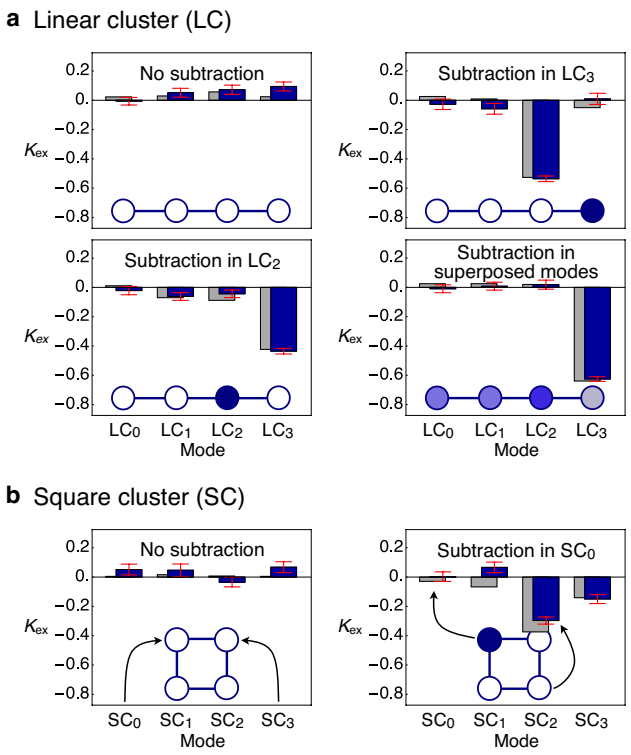

FIG. 3. **Effect of photon subtraction on cluster states.** (a) A linear and (b) a square cluster state. K_{ex}, defined in Eq. (2), is the excess kurtosis of quadrature outcomes by randomizing the phase information, where $K_{\mathrm{ex}} < 0$ indicates a non-Gaussian quantum state. For the photon subtraction in the superposed modes (bottom right in (a)), we use $-0.4i\mathrm{LC}_0 - 0.4\mathrm{LC}_1 + 0.8i\mathrm{LC}_2 + 0.2\mathrm{LC}_3$. Blue bars are experimental data, where each error bar represents one standard deviation of the mean. Gray bars are theoretical predictions, which are obtained by applying an ideal photon subtraction (or no photon subtraction) to the input state based on Extended Data Fig. 3.

METHODS

Experimental details. Non-Gaussian multimode quantum states are generated by several nonlinear interactions on femtosecond pulses, as described in Fig. 1. The fundamental light source is a Ti:Sapphire laser, which produces a train of pulses (duration: 90 fs, central wavelength: 795 nm) at a repetition rate of 76 MHz. The laser beam is split into three beams: one is used for generating a multimode Gaussian state, another for photon subtraction, and the third for the homodyne detection.

The first beam is up-converted to a femtosecond pulse having 397.5-nm central wavelength in NC_1 (0.2-mm-thick BiB_3O_6) which is used as a pump for a parametric-down-conversion process in NC_2 (2-mm-thick BiB_3O_6) inside a cavity, the SPOPO. The length of the SPOPO is locked to the length of the Ti-Sapphire laser via the Pound-Drever-Hall method, such that the train of pump pulses is synchronized with the down-converted pulses which circulate inside the SPOPO. Transmittance of the output coupler of the SPOPO is 50%. The light coming out through the output coupler is a multimode Gaussian state, containing roughly twelve squeezed vacua in orthogonal time-frequency modes [4, 29]. Among the twelve modes, we focus on the first four dominating modes, whose covariance matrix is given in Extended Data Fig. 3.

For photon subtraction, we perform sum-frequency interaction between the multimode Gaussian state and the second beam from the Ti-Sapphire laser (the gate; 1 mW power) inside NC_3 (2.5-mm-thick BiB_3O_6). Detection of a single photon generated by the sum-frequency interaction heralds photon subtraction from the multimode squeezed vacua, where the time-frequency mode of the gate determines the photon subtraction mode [30]. To engineer the time-frequency mode of the gate, we employ a homemade pulse shaper whose core element is a spatial light modulator, having a spectral resolution of 0.2 nm. Conversion efficiency of the nonlinear interaction is 0.1 %, and we have typically 110 Hz of heralding rate with background noise of 6 Hz.

The last beam is used as the local oscillator (LO) of the homodyne detection to measure the generated quantum state. The measurement mode is the mode of the LO, which is engineered by another pulse shaper having a spectral resolution of 0.2 nm. For each event of photon subtraction, photocurrent difference between the two PDs is sampled every 2 ns during a 2-μs time window, and one quadrature outcome is obtained by calculating the

dot product between the samples and the double-sided-decaying-shape temporal mode of the SPOPO [37]. To reconstruct a Wigner function in Fig. 2, we collect 20,000 $\sim$ 30,000 quadrature outcomes. In the case of no photon subtraction, we monitor the variance of the quadrature outcomes. Phase dependance of the quadrature squeezing of the multimode Gaussian state provides the phase information of the LO relative to this multimode light.

Preparation of entangled states. We prepare an entangled state by choosing a specific basis of modes in which quantum correlations among desired modes emerge [4, 29]. In the HG mode basis, even-order (odd-order) modes exhibit p-quadrature (x-quadrature) squeezed vacuum. To prepare an EPR entangled state, we use a basis of $\mathrm{EPR}_0 = \frac{1}{\sqrt{2}}(\mathrm{HG}_0 + \mathrm{HG}_1)$ and $\mathrm{EPR}_1 = \frac{1}{\sqrt{2}}(\mathrm{HG}_0 - \mathrm{HG}_1)$. We have obtained $\langle\Delta^2(\hat{x}_0^{\mathrm{EPR}} - \hat{x}_1^{\mathrm{EPR}})\rangle + \langle\Delta^2(\hat{p}_0^{\mathrm{EPR}} + \hat{p}_1^{\mathrm{EPR}})\rangle = 2.51(6) < 4$ (the Duan entanglement criterion [38, 39]) and $\langle\Delta^2\hat{x}_{1|0}^{\mathrm{EPR}}\rangle\langle\Delta^2\hat{p}_{1|0}^{\mathrm{EPR}}\rangle = 0.71(4) < 1$ (the EPR criterion [40]). To prepare a linear cluster state, we use a basis of LC_k ($k = 0, 1, 2, 3$) which is obtained by applying a unitary matrix $U^{(\mathrm{LC})}$ to the basis of HG_k ($k = 0, 1, 2, 3$), where

$$U^{(\mathrm{LC})} = \begin{pmatrix} -0.344i & -0.421i & 0.531i & 0.650i \\ 0.344 & -0.765 & -0.531 & 0.119 \\ -0.765i & -0.344i & -0.119i & -0.531i \\ 0.421 & -0.344 & 0.650 & -0.531 \end{pmatrix}.$$

To check correlations among different modes, we use the four nullifiers associated with a linear cluster state [29, 41], $\hat{\delta}_k^{(\mathrm{LC})} = \hat{x}_k - \sum_l V_{kl}\hat{p}_l$ (V_{kl} is the adjacency matrix defining the topology of a cluster state, where $V_{kl} = 1$ if k and l are connected, and 0 otherwise). They all exhibit a variance less than the vacuum fluctuation: $\langle\Delta^2\hat{\delta}_k^{(\mathrm{LC})}\rangle / \langle\Delta^2\hat{\delta}_k^{(\mathrm{LC})}\rangle_{\mathrm{vacuum}} = 0.75(2)$, 0.67(2), 0.68(2), and 0.64(2) for $k = 0$, 1, 2, and 3, respectively. Similarly, we prepare a square cluster state in the basis of SC_k ($k = 0, 1, 2, 3$), which is obtained by applying a unitary matrix $U^{(\mathrm{SC})}$ to the HG basis, where

$$U^{(\mathrm{SC})} = \begin{pmatrix} -0.316 & 0.632 & 0.707 & 0.000 \\ 0.632i & 0.316i & 0.000 & -0.707i \\ -0.316 & 0.632 & -0.707 & 0.000 \\ 0.632i & 0.316i & 0.000 & 0.707i \end{pmatrix}.$$

Each of the four nullifiers $\hat{\delta}_k^{(\mathrm{SC})}$ associated with a square cluster state exhibits a variance less than the vacuum fluctuation: $\langle\Delta^2\hat{\delta}_k^{(\mathrm{SC})}\rangle / \langle\Delta^2\hat{\delta}_k^{(\mathrm{SC})}\rangle_{\mathrm{vacuum}} = 0.72(2)$, 0.77(2), 0.61(2), and 0.75(2) for $k = 0$, 1, 2, and 3, respectively.

DATA AVAILABILITY

The data that support the plots within this paper and other findings of this study are available from the corresponding author upon reasonable request.

			Subtraction mode		
		Input	HG_0	HG_1	HG_2
Measurement mode	HG_0	0.91(1)	0.45(1) [0.53(2)]	0.88(1)	0.87(1)
	HG_1	0.90(1)	0.82(1)	0.47(1) [0.49(1)]	0.86(1)
	HG_2	0.91(1)	0.87(1)	0.77(1)	0.49(1) [0.50(2)]

Extended Data Table 1. **Purities of the Wigner functions in Fig. 2(a).** For comparison, the purity of a Wigner function by the ideal photon subtraction is provided in square brackets, which agrees well with the experimental result. Low purity in a photon-subtracted mode is attributed to a non-ideal input state [19]. No optical loss is corrected in the calculation. Errors noted in parentheses are one standard deviations calculated by bootstrapping.

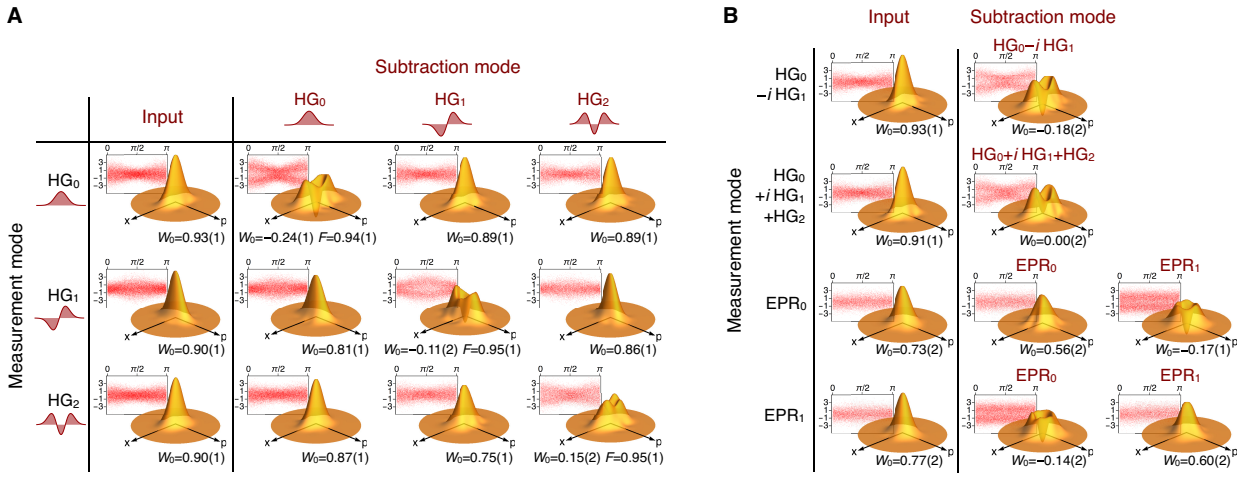

Extended Data Fig. 1. **Wigner function reconstructed with optical loss correction.** Optical loss only by the homodyne detection (12.5%) has been corrected. Comparing with Fig. 2, non-Gaussian Wigner functions show reduced W_0. Errors noted in parentheses are one standard deviations calculated by bootstrapping.

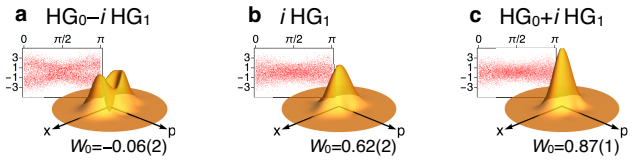

Extended Data Fig. 2. **Effect of mode mismatch between photon subtraction and measurement.** When a single photon is subtracted in $\mathrm{HG}_0 - i\mathrm{HG}_1$, a Wigner function (without optical loss correction) is obtained in a measurement mode having (a) full match ($\mathrm{HG}_0 - i\mathrm{HG}_1$), (b) partial match ($i\mathrm{HG}_1$), and (c) no match ($\mathrm{HG}_0 + i\mathrm{HG}_1$). Errors noted in parentheses are one standard deviations calculated by bootstrapping.

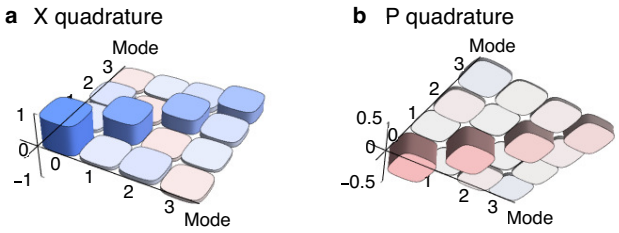

Extended Data Fig. 3. **Experimental covariance matrix.** (a) is for x quadratures, seen from above, and (b) is for p quadratures, seen from below. Mode indexes are HG_0, $i\mathrm{HG}_1$, HG_2, and $i\mathrm{HG}_3$, where i is added for the odd-index HG modes to have p-squeezed vacua in all modes. For clarity, the vacuum noise (corresponding to the identity matrix) is subtracted from the covariance matrix. In the covariance matrix, variances of (x, p) quadratures are (2.8 dB, −1.8 dB) in mode 0, (2.1 dB, −1.6 dB) in mode 1, (1.6 dB, −1.0 dB) in mode 2, and (1.4 dB, −0.7 dB) in mode 3.